Zinc Sulfide Nanoparticle-decorated Fibre Mesh to Enable Localized H2S-amplified Chemotherapy

DOI:
10.1039/D0CC00763C

Document Version
Accepted author manuscript

ChemComm
Chemical Communications

Accepted Manuscript

This article can be cited before page numbers have been issued, to do this please use: G. Wang, D. Cen, Z. Ren, Y. Wang, X. Cai, X. Chen, X. Li, S. M. Best and G. Han, *Chem. Commun.*, 2020, DOI: 10.1039/D0CC00763C.

ROYAL SOCIETY OF CHEMISTRY

rsc.li/chemcomm

View Article Online
DOI: 10.1039/D0CC00763C

Journal Name

COMMUNICATION

Zinc Sulfide Nanoparticle-decorated Fibre Mesh to Enable Localized H_2S-amplified Chemotherapy

Received 00th January 20xx,
Accepted 00th January 20xx

DOI: 10.1039/x0xx00000x

Gang Wang [†a], Dong Cen [†b], Zhaohui Ren [a], Yifan Wang [b], Xiujun Cai [b], Xiaohui Chen [c], Xiang Li *[a], Serena Best [d], Gaorong Han *[a]

For the first time, we report the design and fabrication of a ZnS nanoparticle-decorated silica fibre mesh (ZnS@SiO_2) for localized H_2S-amplified chemotherapy. With incorporation of DOX, implanted ZnS@SiO_2 fibres enable sufficient on-site drug dosage and intracellular H_2S content, inducing significant *in vitro* and *in vivo* tumour inhibition.

While current systemic drug delivery systems (SDDSs) for chemotherapy still face challenges such as burst drug release, low targeting efficiency and inevitable clearance during circulation [1,2]. Localized drug delivery systems (LDDSs), in forms of films, hydrogels, microarrays, rods or drug-eluting wafers, have been developed for targeted chemotherapy [3, 4]. Electrospun fibres offer the potential for superior performance in localized chemotherapy due to their unique properties such as high surface area, flexibility and so on [5-7]. Additional benefits include sustained and continuous release of chemotherapeutic drugs, providing a high local drug concentration at the tumour site while maintaining a low drug level in the biological system. For this reason, intensive research has been carried out on fibre-based LDDSs for chemotherapy [1], and recently there was a move towards drug-loaded nanoparticle-fibre assemblies, in which nanoparticles can be taken-up by cancer cells, underwent intracellular drug release. Meanwhile, there has been rapid advances in nanomedicine and nanotechnology for more efficient anticancer purposes. Among these emerging modalities, gas therapy has been explored utilizing the generation of therapeutic gases [8] such as nitric oxide (NO) [9], carbon monoxide (CO) [10], hydrogen (H_2) [11] and hydrogen sulfide (H_2S) [12, 13] to induce cell death. As the third gas transmitter after NO and CO [14]. H_2S can be generated endogenously by the catalysis of H_2S-producing enzymes [15]. Endogenous or low levels of H_2S may lead to pro-cancer effects while the presence of high H_2S levels may induce cancer inhibition [16]. Interestingly, studies also suggested that excessive H_2S can increase the oxidative stress build-up in cancer cells by suppression of the enzyme catalase (CAT) [17]. In addition, ZnS can actively react with H^+ in the acid environment, and thus offers the potential for effective H_2S generation [18, 19]. Meanwhile, doxorubicin (DOX), a broad-spectrum drug used in chemotherapy, could also induce the generation of reactive oxygen species (ROS) besides its capability in causing cancer cell DNA dysfunction [20]. The suppression of CAT leads to over-production of H_2O_2, increasing the ROS level and promoting DNA damage and cell necrosis [21]. Therefore, it would be logical to combine DOX and H_2S gas in one therapeutic platform to achieve H_2S-enhanced chemotherapy. However, to the best of our knowledge, no such investigation has yet been reported.

[a] State Key Laboratory of Silicon Materials, School of Materials Science and Engineering, Zhejiang University, 310027, China. E-mail: xiang.li@zju.edu.cn; hgr@zju.edu.cn
[b] Department of General Surgery, Institute of Minimally Invasive Surgery, Sir Run Run Shaw Hospital, College of Medicine, Zhejiang University, 310016, China
[c] Division of Dentistry, School of Medical Sciences, The University of Manchester, UK, Manchester, M13 9PL, UK
[d] Department of Materials Science and Metallurgy, University of Cambridge, Cambridge CB3 0FS, UK
† Authors with equal contribution.

Electronic Supplementary Information (ESI) available: N_2 absorption and desorption isotherm curves of SiO_2 fibres and ZnS@SiO_2 fibres. TEM images of ZnS nanoparticles released from ZnS@SiO_2 fibres. DOX loading efficiency and capacity of ZnS@SiO_2 fibres. SEM images of ZnS@SiO_2 fibres after incubation with PBS solution at pH=5.4 for different time. Bright field images of Huh7 cells after incubation with various samples at pH = 6.0 for 12 h. Photographs of representative mice after treatment. See DOI: 10.1039/x0xx00000x

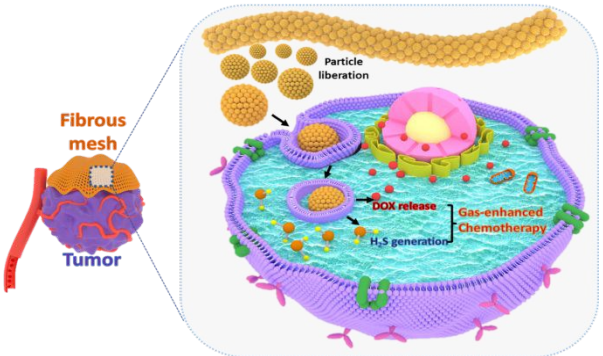

Fig. 1 Schematic illustration of DOX-ZnS@SiO_2 fibrous mesh for localized H_2S-amplified chemotherapy.

View Article Online
DOI: 10.1039/D0CC00763C

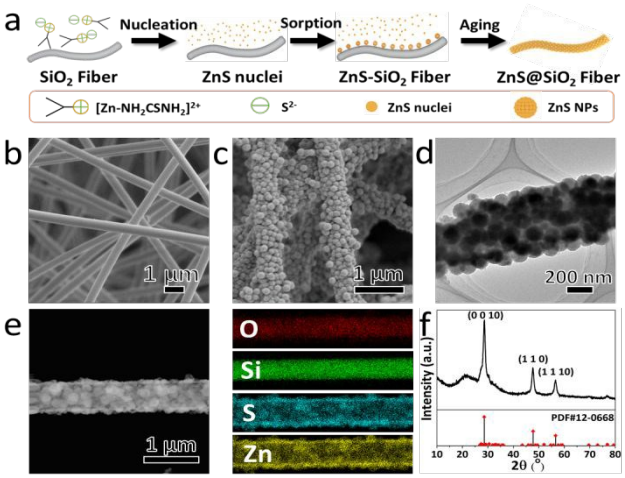

Fig. 2 (**a**) Schematic illustration of the formation mechanism of ZnS@SiO_2 fibres; SEM images of (**b**) as-spun SiO_2 and (**c**) ZnS@SiO_2 fibres; (**d**) TEM image, (**e**) EDS elemental mapping and (**f**) XRD pattern of ZnS@SiO_2 fibres.

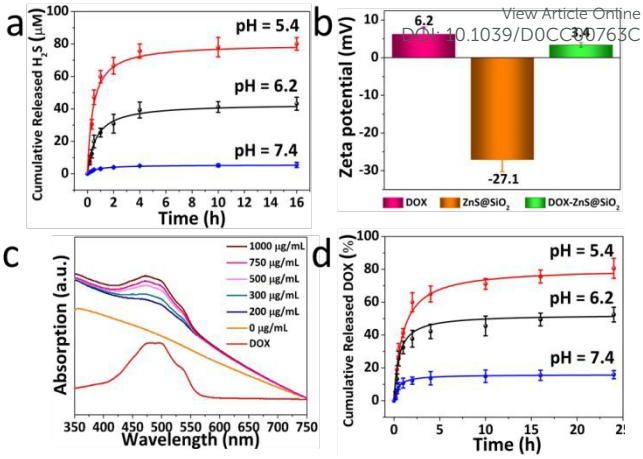

Fig. 3 (**a**) Cumulative H_2S gas release of ZnS@SiO_2 fibrous mesh in solutions different pH; (**b**) Zeta potentials of DOX, ZnS@SiO_2 fibres and DOX-ZnS@SiO_2 fibres; (**c**) UV-Vis spectra of DOX solution, ZnS@SiO_2 fibres and DOX-ZnS@SiO_2 fibres loaded in DOX solutions with different concentrations; (**d**) Cumulative DOX release profile of DOX-ZnS@SiO_2 fibres in PBS at different pH values.

In the present study, we aimed to develop an enhanced chemotherapy platform combining the benefits of both gas therapy and localized drug release, comprising doxorubicin (DOX) loaded ZnS nanoparticles assembled silica fibres (DOX-ZnS@SiO_2) (as shown in **Fig. 1**). The *in vitro* and *in vivo* anticancer performance of the DOX-ZnS@SiO_2 fibrous mesh was also revealed.

ZnS@SiO_2 composite fibres were synthesized via hydrothermal growth of ZnS nanoparticles on the surface of silica nanofibres (procedure as demonstrated in **Fig. 2a**). A flexible silica fibrous membrane was prepared via electrospinning and subsequent heat treatment according to a modified sol-gel method reported previously [22]. After calcination at 800°C for 3 h, the as-prepared SiO_2 nanofibres presented a fibrous texture and smooth surface morphology (**Fig. 2b**). Flexible silica nanofibres with negative charged surface and inactivity during hydrothermal process enabled the assembly of ZnS nanoparticles [23].

Following the hydrothermal synthesis of ZnS nanoparticles reported previously [24], ZnS nuclei formed in the precursor solution, and were subsequently absorbed and grew on the surface of silica fibres. ZnS nanoparticles with an average diameter of ~110 nm were uniformly assembled on the surface of silica fibres (**Fig. 2c**, **2d**). In consequence, the diameter of the composite fibres increased from 510 nm to 720 nm, and a slight decrease in surface area was observed (**Fig. S1**). ZnS nanoparticles liberated from ZnS@SiO_2 fibres were composed of nanocrystals, which increased the pore size of the composite fibres (**Fig. S2**). Meanwhile, element mapping images showed a homogeneous distribution of sulphur and zinc in ZnS@SiO_2 composite fibres (**Fig. 2e**), confirming the successful growth of ZnS nanoparticles on the surface of silica nanofibres. A representative XRD pattern of the as-prepared ZnS@SiO_2 composite fibres is shown in **Fig. 2f**. The broad peak appeared from 15° to 35° on the diffraction pattern was ascribed to SiO_2 due to its amorphous nature. Three main diffraction peaks are visible and these match well with the primary peaks of the characteristic diffraction patterns of wurtzite ZnS (PDF# 12-0688), indicating the assembly of ZnS on the surface of SiO_2 nanofibres. The ZnS@SiO_2 composite fibres synthesized demonstrated a high degree of ZnS nanoparticle loading, and this laid the foundation for the construction of a H_2S-enhanced chemotherapy platform.

The *in vitro* H_2S gas release profile of the ZnS@SiO_2 composite fibres was investigated at different pH values. The concentration of H_2S gas in aqueous solution was measured using a spectrophotometric procedure and quantified with a standard curve (**Fig. S3**). Under neutral conditions, the mean cumulative concentration of H_2S gas was 4.9 μM after the first 4 h and 5.5 μM after 16 h. In comparison, under acidic conditions (designed to simulate the mild acid tumour microenvironment) the mean cumulative concentration of H_2S after 16 h reached 43.3 μM and 80.6 μM at pH = 6.2 and pH = 5.4, respectively (**Fig. 3a**). These results demonstrate that, in the presence of hydrogen ions (H^+), ZnS nanoparticles on the surface of ZnS@SiO_2 composite fibres could react with H^+ to produce H_2S gas which is a prerequisite for H_2S-enhanced chemotherapy.

Encouraged by the favourable structure of ZnS@SiO_2 fibres, DOX was used as a model drug and loaded on the fibrous mesh for chemotherapy. As shown in **Fig. 3b**, the mean zeta potentials of DOX and ZnS@SiO_2 fibres were 6.2 mV and -27.1 mV, implying that it is feasible to load DOX by electrostatic absorption. After drug loading, the mean zeta potential of DOX-ZnS@SiO_2 fibres became positive (3.4 mV), indicating the successful loading of DOX. UV-Vis spectra of DOX loaded ZnS@SiO_2 composite fibres (**Fig. 3c**) revealed that the DOX loading capacity increased with the increasing DOX concentration, while the loading efficiency decreased sharply (**Fig. S5**). Considering the adverse effects and therapeutic effects [25], the loading concentration of DOX solution was set at 100 μg/ml for subsequent studies.

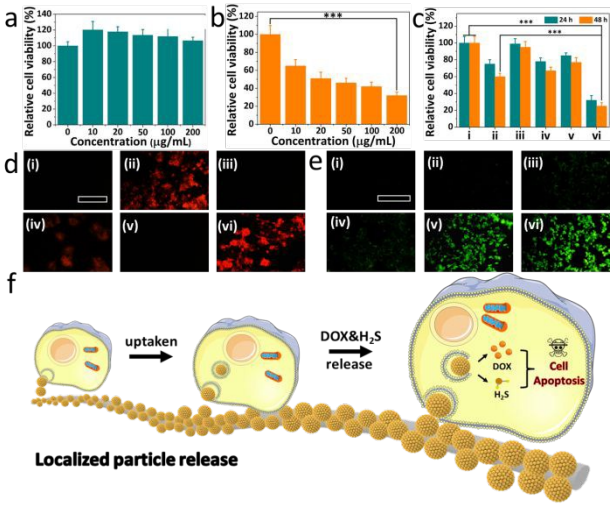

Fig. 4 Relative viability of (**a**) 7702 cells incubated with ZnS@SiO_2 fibres for 24 h at pH = 7.4 and (**b**) Huh7 cancer cells incubated with DOX-ZnS@SiO_2 fibres with different concentrations at pH = 6.0 for 24 h; (**c**) Relative cell viability, (**d**) DOX fluorescent images and (**e**) WSP-1 fluorescent images of Huh7 cancer cells incubated with (i) pure culture medium, (ii) DOX (4.5 μg/mL), (iii) ZnS@SiO_2 fibres (100 μg/mL) at pH = 7.4, (iv) DOX-ZnS@SiO_2 fibres (100 μg/mL) at pH = 7.4, (v) ZnS@SiO_2 fibres at pH = 6.0, (vi) DOX-ZnS@SiO_2 fibres at pH = 6.0. Scale Bar: 100 μm; (**f**) Mechanism illustration of the H_2S-enhanced anticancer effect achieved by DOX-ZnS@SiO_2 fibres.

The *in vitro* DOX release profile of DOX-ZnS@SiO_2 composite fibres was investigated (**Fig. 3d**). At pH = 7.4, only 15.9% of DOX was released in the initial 24 h, which could be attributed to free diffusion of DOX in the composite fibres. In contrast, 80.6% and 52.4% of DOX in the composite fibres were released in the same period at pH = 5.4 and pH = 6.2, respectively. There are two reasons for the pH-dependent release profile. As discussed previously, under acidic conditions, ZnS nanoparticles react with H^+ ions to release H_2S gas. As the reaction proceeds, it is suggested that the ZnS nanoparticles are liberated from silica fibres (**Fig. S6**). The hydrodynamic diameter of the release ZnS nanoparticles was ~190 nm with polymer dispersion index of 0.289 (**Fig. S7**). Moreover, H^+ ions are likely to destroy the electrostatic interaction between ZnS nanoparticles and DOX molecules, also accelerating the drug-release.

The *in vitro* performance of DOX-ZnS@SiO_2 composite fibres was investigated using Human HL-7702 liver cells and Human Huh-7 liver cancer cells. As shown in **Fig. 4a**, no clear toxicity was observed when the concentration of ZnS@SiO_2 fibre was increased up to 200 μg/ml, indicating its biocompatible. This observation was thought to be due to the fact that, under neutral conditions, the concentration of H_2S released from ZnS@SiO_2 fibres is not sufficiently high to induce normal cells death. To uncover the anticancer performance, Huh7 liver cancer cells were incubated with DOX-ZnS@SiO_2 fibres under different concentrations. The pH of the culture media was adjusted to 6.0 by adding hydrochloric acid [26]. Incubation for 24 h at concentration of DOX-ZnS@SiO_2 fibres up to 200 μg/ml resulted in 68.2% Huh7 cell death and the IC50 value was ~23.6μg/ml (**Fig. 4b**). To further investigate the underlying

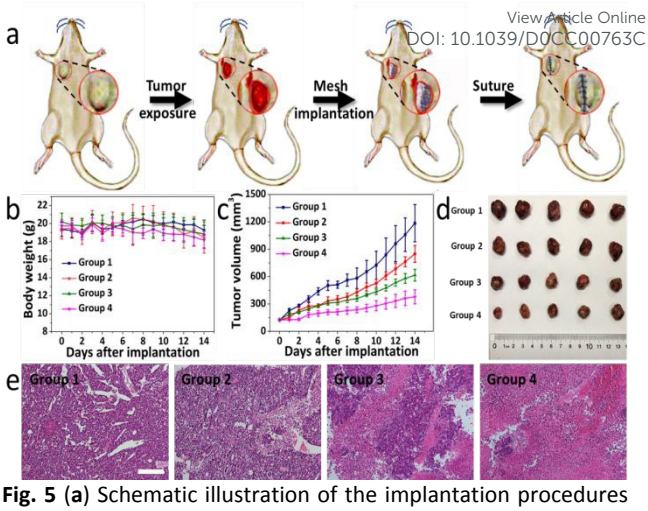

Fig. 5 (**a**) Schematic illustration of the implantation procedures of DOX-ZnS@SiO_2 fibres at the tumor site; (**b**) body weight and (**c**) tumor volume variations of mice after various treatments (n=5); Digital photographs of (**d**) representative tumors and (**e**) H&E-stained tumor slices collected from different groups of mice after 14-day treatment. Scale bar: 1000 μm

influence of H_2S gas induced, the following systems were used to treat Huh7 cells: (i) pure culture medium; (ii) culture medium containing DOX of 4.5 μg/mL; (iii) ZnS@SiO_2 fibres of 100 μg/mL at neutral pH; (iv) DOX-ZnS@SiO_2 fibres of 100 μg/mL at neutral pH; (v) ZnS@SiO_2 fibres of 100 μg/mL at pH =6.0; (vi) DOX-ZnS@SiO_2 fibres of 100 μg/mL at pH = 6.0. The concentration of DOX in Group (ii) maintained at the same level as that for the DOX-ZnS@SiO_2 fibres in Group (iv) and Group (vi). However, it should be noted that this is relatively low in comparison with that reported in DOX chemotherapy [23]. As shown in **Fig. 4c**, after 48 h incubation, for free DOX alone (ii) only 39.5% Huh7 cell death occurred, and ZnS@SiO_2 fibres induced virtually no cell necrosis under neutral pH condition. In comparison, although certain H_2S gas may potentially release extracellularly, the cell viability (Group v) decreased to ~77.1% after incubation with ZnS@SiO_2 fibres at pH = 6.0 for 48 h. This could be attributed to the release of high concentrations of on-site H_2S gas in the acidic environment, consequently inducing cell death. The cell viability of DOX-ZnS@SiO_2 fibres decreased from ~68.6% (Group iv) to ~24.8% (Group vi) after 48 h when the culture medium varied from the neutral to pH=6, implying its amplified *in vitro* anticancer performance by the H_2S induced in an acid condition.

The examination using flow cytometry indicates that the tumour cell can effectively uptake ZnS nanoparticles released from the composite fibres during the incubation for 24 h (**Fig. S8**). The synergistic anticancer performance of the DOX-ZnS@SiO_2 fibre mesh, was investigated by evaluating the intracellular presence of DOX and H_2S. Under excitation at 480 nm, DOX presents intense red fluorescence at 590 nm. After 12 h incubation, as expected, Huh7 cells treated with the DOX-ZnS@SiO_2 fibrous mesh at pH=6.0 showed higher intracellular level of DOX even than those treated with pure DOX (**Fig. 4d, Fig. S9**). This may be associated with the continuous release of DOX from the DOX loaded fibres under acidic conditions, while pure DOX was consumed rapidly during the incubation process. In addition, using WSP-1 as a probe, cells incubated with

$ZnS@SiO_2$ and DOX-$ZnS@SiO_2$ fibres encountered significant H_2S gas release under acidic conditions (**Fig. 4e, Fig. S10**). On the contrary, no H_2S gas was released under neutral pH conditions.

Based on the *in vitro* findings, it is proposed that, under an acidic condition, DOX-loaded ZnS nanoparticles on the surface of silica fibres are released and taken-up by Huh7 cells. Subsequently, both DOX and H_2S gas are released intracellularly. The H_2S at the certain concentration may amplify the anticancer efficacy of DOX (**Fig. 4f**). This is attributed to that H_2S gas can effectively suppress the activity of catalase which is the key enzyme for H_2O_2 decomposition [26]. Thus, increased oxidative stress at the tumour site leads to cell apoptosis and improved efficacy of DOX.

The *in vivo* therapeutic performance of DOX-$ZnS@SiO_2$ fibre mesh was investigated using a Huh7 mouse tumour model. $ZnS@SiO_2$ fibres and DOX-$ZnS@SiO_2$ fibres were implanted in the tumour site via minimally invasive surgery, respectively (**Fig. 5a**). Compared with the control group (Group 1), no clear weight variation was observed in the mice treated with intratumorally injected DOX (Group 3), $ZnS@SiO_2$ fibres (Group 2) and DOX-$ZnS@SiO_2$ fibres (Group 4), indicating that there was no acute toxicity associated with the treatment systems (**Fig. 5b**). On day 14, the tumour progression of mice treated with low dosage of DOX was partially inhibited (**Fig. 5c**). Mice treated with $ZnS@SiO_2$ fibres showed considerable tumour suppression compared with the control group (**Fig. S11 and Fig. 5d**). However, for those treated with DOX-$ZnS@SiO_2$ fibrous mesh, the tumour sizes shrank after 14 days treatment. Furthermore, H&E-stained microscopy slices of tutors indicated that the tumour tissues treated with DOX-$ZnS@SiO_2$ fibres were more seriously damaged than those with DOX only (**Fig. 5e**). However, in the control groups with $ZnS@SiO_2$ fibres, the tumour tissues retained their normal pathology. Overall, the *in vivo* results suggest that the use of a DOX-$ZnS@SiO_2$ fibre mesh offers an effectively enhanced chemotherapeutic efficacy.

In this study, for the first time, a fibrous silica mesh with an active surface comprising ZnS nanoparticles is synthesized to enable H_2S gas combined chemotherapy in a localized manner. ZnS nanoparticles, used as a H_2S-generating donor, were assembled on the surface of electrospun SiO_2 nanofibres. Under acidic conditions, $ZnS@SiO_2$ nanofibres released H_2S gas due to the reaction of ZnS with H^+ ions. The cumulative H_2S gas concentration was up to 80.63 μM at pH= 5.4, which was significantly higher than that in normal tissue. ZnS nanoparticles may liberate from $ZnS@SiO_2$ fibres in the presence of H^+ ions and can be effectively taken-up by cancer cells. The DOX loaded $ZnS@SiO_2$ fibres exhibited a pH-dependent drug release profile. The *in vitro* study demonstrated that, due to the combined effects for intracellular DOX and H_2S induction, DOX-$ZnS@SiO_2$ fibres had exceptional *in vitro* and *in vivo* performance when compared with pure DOX or $ZnS@SiO_2$ fibres. This study offers a distinctive approach to materials design by combining fibres and particles for LDDSs and will pave the way not only for enhanced chemotherapy, but also other modalities of ROS-based cancer treatment.

Acknowledgement

View Article Online
DOI: 10.1039/D0CC00763C

This work was financially supported by National Nature Science Foundation of China (51672247), ZJU-Hangzhou Global Scientific and Technological Innovation Center, '111' Program funded by Education Ministry of China and Sate Bureau of Foreign Experts Affairs (B16043), Fundamental Research Funds for the Central Universities (2019XZZX005-3-01) and Provincial Key Research Program of Zhejiang Province (2020C04005).

Conflicts of interest

There are no conflicts to declare.

Notes and references

1 Y. Fu, X. Li, Z. Ren, C. Mao and G. Han, Small, 2018, 14, 1801183.
2 H.-K. Yang, J.-F. Bao, L. Mo, et. al., RSC Adv., 2017, 7, 21093-21106.
3 L. Polakova, J. Sirc, R. Hobzova, A. I. Cocarta and E. Hermankova, International journal of pharmaceutics, 2019, 558, 268-283.
4 J. B. Wolinsky, Y. L. Colson and M. W. Grinstaff, J. Controlled. Release, 2012, 159, 14-26.
5 J. Xue, J. Xie, W. Liu and Y. Xia, Accounts Chem Res, 2017, 50, 1976-1987.
6 S. Jiang, L. P. Lv, K. Landfester and D. Crespy, Accounts Chem Res, 2016, 49, 816-823.
7 L. S. Nair, S. Bhattacharyya and C. T. Laurencin, Expert Opin Biol Th, 2004, 4, 659-668.
8 H. Lin, Y. Chen and J. Shi, Chem Soc Rev, 2018, 47, 1938-1958.
9 X. Zhang, G. Tian, W. Yin, et. al., Adv. Funct. Mater., 2015, 25, 3049-3056.
10 Y. Wang, Z. Liu, H. Wang, et. al., Acta Biomater, 2019, 92, 241-253.
11 I. Ohsawa, M. Ishikawa, K. Takahashi, et. al., Nature Med, 2007, 13, 688-694.
12 G. L. Bannenberg and H. L. Vieira, Expert Opin Ther Pat, 2009, 19, 663-682.
13 Z. W. Lee, J. Zhou, C. S. Chen, Y. Zhao, C. H. Tan, L. Li, P. K. Moore and L. W. Deng, PloS one, 2011, 6, e21077.
14 K. Abe, H. Kimura, J Neurosci, 1996, 16, 1066–1071.
15 B. L. Predmore, D. J. Lefer and G. Gojon, Antioxid & Redox Sign, 2012, 17, 119-140.
16 M. R. Hellmich, C. Coletta, C. Chao and C. Szabo, Antioxid & Redox Sign, 2015, 22, 424-448.
17 M. A. Eghbal, P. S. Pennefather and P. J. O'Brien, Toxicology, 2004, 203, 69-76.
18 S. Licht, J. Electrochem. Soc., 1988, 135, 2971-2975.
19 S. K. Dash, T. Ghosh, S. Roy, S. Chattopadhyay and D. Das, Journal of applied toxicology : JAT, 2014, 34, 1130-1144.
20 Y. Chen, P. Jungsuwadee, M. Vore, D. A. Butterfield and D. K. St Clair, Molecular interventions, 2007, 7, 147-156.
21 M. S. Attene-Ramos, E. D. Wagner, H. R. Gaskins and M. J. Plewa, Molecular cancer research : MCR, 2007, 5, 455-459.
22 X. Mao, Y. Si, Y. C. Chen, L. P. Yang, F. Zhao, B. Ding and J. Y. Yu, RSC Adv., 2012, 2, 12216-12223.
23 G. Wang, Y. Fu, Z. Ren, J. Huang, S. Best, X. Li and G. Han, Chem Commun, 2018, 54, 6324-6327.
24 L. Zhang, R. Dong, Z. Zhu et. al., Sensor Actuat B-Chem, 2017, 245, 112-121.
25 W. Zhang, Z. Guo, D. Huang et. al., Biomaterials, 2011, 32, 8555-8561.
26 C. Xie, D. Cen, Z. Ren et. al., Advanced science, 2020, 1903512.